Correlations in a many-body calculation of ^{11}Li

C. R. Chinn
Department of Physics and Astronomy, Vanderbilt University, Nashville, Tennessee 37235

J. Dechargé and J.-F. Berger
Service de Physique et Techniques Nucléaires, Centre d'Etudes de Bruyères-le-Châtel, B.P. No. 12, 91680 Bruyères-le-Châtel, France

(Received 3 August 1994)

A many-body calculation of ^{11}Li is presented where the only input is the well-tested, finite-range *D1S* effective interaction of *Gogny*. The nucleus ground state is modeled as a generator coordinate method configuration mixing of Hartree-Fock-Bogolyubov states generated with a constraint on the mean square radius. Pairing correlations are computed from the two-body interaction itself. The kinds of correlations included in this way are found to play an important role in describing the large ^{11}Li radius. A substantive underlying ^{9}Li core of ^{11}Li is found, which has a different density profile than a free ^{9}Li nucleus. The relations of this work with other approaches are discussed.

PACS number(s): 21.60.Ev, 27.20.+n, 21.10.Gv

I. INTRODUCTION

With the recent advent of secondary beam facilities there has been a large research interest in nuclei near the drip lines. These exotic nuclei offer opportunities to study many-body effects under unusual conditions. An example of such can be related to the nucleon-nucleon [*N*-*N*] interaction. While the free *N*-*N* interaction appears to be well understood, the role of the *N*-*N* interaction in microscopic nuclear structure is far from being clear. (One example where one would think that the role of the *N*-*N* interaction should be clear but is not is in the ^{3}H problem.) Because nuclei near the drip line have weak binding energies and hence large density distributions, the *N*-*N* interaction can now be studied in regions of low nuclear density.

The free neutron-neutron [*n*-*n*] interaction is attractive, but the dineutron system is unbound. Migdal and Watson postulated the possibility that a dineutron may become bound if placed within the field of a nucleus. ^{11}Li among others appears to be such a system, since both ^{11}Li and ^{9}Li are bound while ^{10}Li is not. Hence, with this in mind, recent interest in ^{11}Li has been strongly addressed within a three-body framework [1–6], where ^{11}Li is represented as two neutrons surrounding an inert ^{9}Li core. For a recent review of such work, please see Ref. [1].

The assumption that ^{11}Li can be realistically represented as a three-body system is physically appealing and is confirmed by recent experimental evidence [7,8]. However, in view of the peculiar structure of halo nuclei, it is worthwhile to test other approaches that have been extensively used in the past for "normal" nuclei. Interesting ones are those based upon many-body theory, since they obviate the difficulties that may arise within the three-body framework, such as the approximate treatment of the Pauli exclusion principle and the absence of correlations within the ^{9}Li core.

The most straightforward way to study ^{11}Li in an *A*-body framework is to use the Hartree-Fock approximation, but this was shown for this nucleus [9] to give an inadequate description. By renormalizing the mean field potential, several groups [9–11] found that the experimental two-neutron separation energy and the rms radius of ^{11}Li could be reproduced, thus indicating the possible existence of correlations among the outer single-particle states. Therefore, a description beyond the simple mean field appears to be required. As a first indication of this, a study of pairing correlations using a simple contact force in a three-body calculation showed that such correlations were necessary to bind the two valence neutrons [12]. Correlations on a much larger scale have more recently been included in several conventional shell model descriptions employing up to $3\hbar\omega$ excitations [13,14]. An effect much smaller than the one expected on the ^{11}Li matter radius is generally found. The usual interpretation of this result is that the adopted shell model space is not large enough [13].

In this paper we introduce long-range correlations by using a generator coordinate method (GCM) type formalism. The nuclear ground state (GS) is represented as a superposition of Hartree-Fock-Bogolyubov (HFB) nuclear states, which are obtained by constraining on different values of the $\langle r^2 \rangle$ collective variable. The reason for choosing this particular GCM variable can be understood in the following way: correlations in the ^{11}Li GS are expected to occur because the loosely bound outer neutrons can occupy a large number of nearly degenerate Rydberg-type orbits having a broad range of radial extensions. One expects that a constraint imposing different values of the total rms radius will act essentially on the outer neutron's radial distributions and therefore will be able to generate the kind of configurations present in the nuclear GS. Therefore, as is usual in GCM calculations, initially, a series of constrained HFB microscopic mean field calculations is performed. In a second step the coefficients of the GCM configuration mixing are computed by solving the coupled equations resulting

from the application of a variation principle to the total nucleus binding energy. In the present work, this is accomplished in an approximate fashion by reducing the usual Hill-Wheeler equations to a collective Schrödinger equation of the Bohr type [15]. Note that this calculation includes pairing correlations as well as long-range collective degrees of freedom as derived from the effective N-N interaction. Also, the Pauli principle is strictly obeyed through the use of fully antisymmetrized nuclear states throughout the whole calculation.

The only input into this consistent A-body calculation is the well-tested *D1S Gogny* force. This interaction is a density-dependent phenomenological parametrization of the N-N interaction inside the nuclear medium which includes a spin-orbit term, and is finite-ranged. The parameters of the interaction have been fixed by matching the bulk properties of nuclear matter and of a few finite nuclei, including pairing correlation strengths. This *D1S* force has been tested in a variety of applications with excellent results [16, 17]. It must be noted that this force gives a very good description not only of medium and heavy nuclei, but also of very light nuclei. For instance it describes correctly the binding energy and radius of the alpha particle. In addition the finite-range, density-independent part of the force has been set up in order to roughly simulate a free N-N interaction in the sense that it gives the correct N-N scattering lengths. These properties are important in the present context which deals with a three-proton system where almost free neutron-neutron interactions are expected to play a crucial role.

With this collective model a qualitative study of correlations in ^{11}Li is presented. In particular the role of the ^{9}Li core is explored, especially its relation to a free ^{9}Li nucleus. The validity of the three-body hypothesis is investigated using a collective A-body model.

In Sec. II the mean field constrained and unconstrained HFB calculation is described and the results presented. Long-range correlations using a simplification of the GCM is described in Sec. III along with the results and analysis, followed by a conclusion.

II. CONSTRAINED HFB CALCULATION

The constrained HFB A-body calculation is performed using a 19-shell axially symmetric harmonic oscillator (HO) basis. In performing tests of the convergence of the basis, it was found that a 19-shell basis is required due to the large extension of the neutron matter distribution from the center of the nucleus in coordinate space, and to the inadequate asymptotic behavior of HO states in r space. The use of a multioscillator basis, i.e., of a basis composed of several sets of concentric HO states associated with different lengths, is also used in the HFB calculation. This kind of basis allows one to extend to larger distances the radial description of nucleon orbits. However, in this case only spherically symmetric nuclear distributions could be described. Time-reversal symmetry is assumed, so the protons are described by blocking with equal weights the two $j_z^\pi = \pm 3/2^-$ axial quasiparticle orbitals, thus matching the known ground state spin of both ^{11}Li and ^{9}Li.

For a study of a small nucleus such as ^{11}Li, it would be expected that a mean field description would not be the most appropriate choice. In this case we wish to address certain many-body questions and to test assumptions about the many-body nature of the problem. With this in mind as a first step, a mean field calculation using HFB should be able to address some of these qualitative concerns.

As explained in the Introduction, the ^{11}Li nucleus is expected to be very soft against changes in the density distribution rms. For this reason a constrained HFB calculation was performed, where the constraint variable used corresponds to the mean value of $\langle r^2 \rangle$:

$$q = \int dr\, r^4\, \rho(r) \quad , \text{ where } \rho(r) = \int d\Omega\, \rho(\vec{r}) \, , \qquad (1)$$

$$\langle r_{\rm rms} \rangle = \sqrt{q} \, .$$

When the constraint is switched off, one obtains the mean field representation of the ^{11}Li GS. As mentioned in the Introduction, for a study of such an exotic nucleus as ^{11}Li, the mean field description clearly is not adequate. It is only for the purpose of comparisons with the configuration mixing approach and with the HFB description of ^{9}Li that we comment now on the results of the pure HFB calculation. The total ^{11}Li rms matter radius obtained with HFB is about 2.80 fm, matching the results of several other groups [13, 9]. The separate proton and neutron rms radii are found to be 2.30 and 2.97 fm, respectively. For a similar HFB calculation of the ^{9}Li GS the rms radii are found to be 2.47, 2.24, and 2.58 fm for the total, proton, and neutron distributions, respectively. The rms radii for the protons in ^{9}Li and ^{11}Li differ only by a small amount, resulting from the fact that the three core protons are not greatly affected by the addition of two neutrons. From this we can deduce that, if there is a ^{9}Li core in ^{11}Li, its proton radius will differ from the free ^{9}Li one by roughly the same small amount. Let us already mention that these results concerning the protons will remain unchanged when GCM correlations are introduced. Clearly, very different results are expected for the neutrons. It remains to be seen though how large these differences will be.

In Fig. 1 the results of the constrained ^{11}Li calculation are shown as a function of the constraint variable, q. A similar spherical ^{9}Li calculation is also shown. As q is increased, the ^{11}Li curve is much softer than ^{9}Li in the sense that the slope is much less steep. One then expects ^{11}Li to involve significantly more configuration mixing than ^{9}Li. Such mixing contributions have been included and will be discussed in detail later.

The difference between the unconstrained total binding energies in the ^{11}Li and ^{9}Li calculations gives the mean field HFB value of the two-neutron separation energy, S_{2n}. One finds 910 keV, a value nearly three times larger than the experimental one (340 keV). This is another indication that correlations must play a role, at least in ^{11}Li. Clearly, a much better evaluation of S_{2n} would be to use the GCM lowest ground state energies for both ^{11}Li and ^{9}Li. This is not done in the present work where the

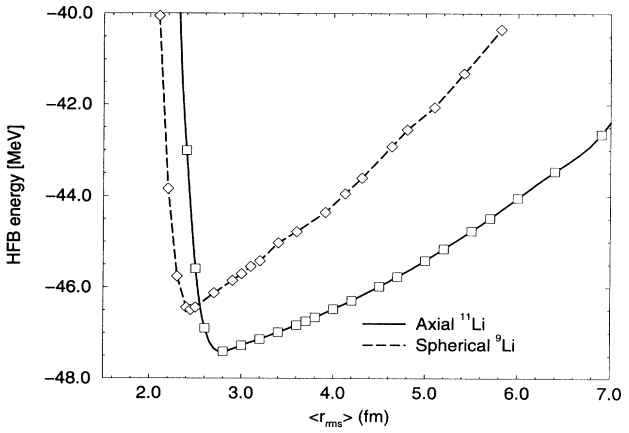

FIG. 1. The total Hartree-Fock-Bogolyubov energy as a function of the constraint variable $\langle r^2 \rangle$ for ^{11}Li and ^{9}Li is shown. The ^{9}Li result is taken from a spherically symmetric HFB calculation.

GCM calculation (a large scale computer one) has been performed only for ^{11}Li. Actually, it is well known that a certain amount of configuration mixing is necessary in light odd nuclei such as ^{9}Li in order to accurately reproduce GS masses, spins, and deformations [18, 13]. For this reason, the HFB calculation of ^{9}Li will be used here only for the purpose of comparing the nucleon density profiles of a free ^{9}Li nucleus with the ^{9}Li core extracted from ^{11}Li. In making this comparison we shall rely on the reasonable assumption that the overall shape of GS density distributions in ^{9}Li is not significantly affected by the configuration mixing present in this nucleus.

The rms radii for the neutron and proton distributions are shown in Fig. 2(a) for the constrained HFB results as a function of $\langle r_{\rm rms} \rangle_{\rm total} = \sqrt{q}$. As expected (see the Introduction) the proton rms is unaffected by the constraint, while the neutron $\langle r_{\rm rms} \rangle_n$ varies linearly. In other words, the curve confirms that the potential between the protons and outer neutrons is not strong enough to prevent the two distributions from decoupling.

The independent nature of the proton and neutron sectors is also evident in the pairing energy shown in Fig. 2(b). The protons consistently have zero pairing as a function of q. The neutrons have strong pairing for $q > 3$ fm indicating the onset of a significantly high neutron level density at the Fermi surface.

Since the protons do not exhibit pairing there must be a sizable gap at the Fermi surface. This is shown in Fig. 3(a), where the protons occupy the $1s$ 1/2 and $1p$ 3/2 states. There is a gap of about 6 MeV between the $1p$ 3/2 level and the higher single-particle levels and this gap remains for all q considered. The relative energies of the occupied levels do not change significantly as a function of q, confirming the negligible influence of the constraint on the proton mean field. Note that, since the $1p$ 3/2 level does not shift a great deal, the blocking approximation used here to account for the odd number of protons should be reasonable.

In Fig. 3(b) the corresponding neutron single-particle

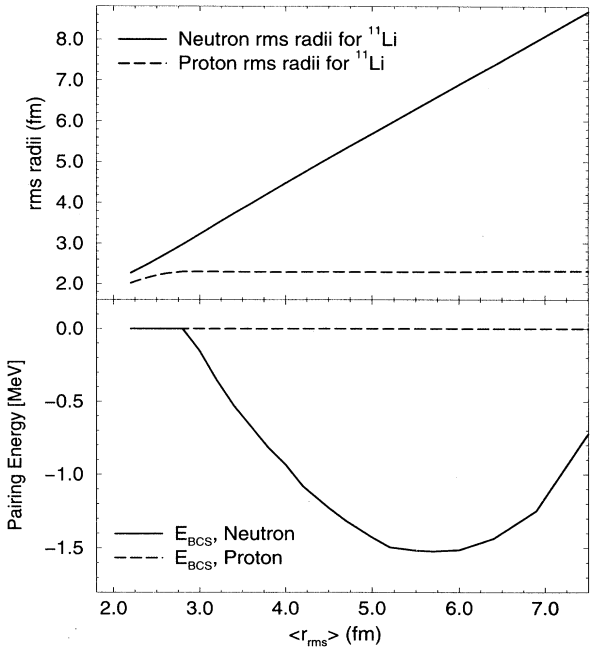

FIG. 2. In the upper panel the separate rms radii for the proton and neutron distributions are plotted for the constrained HFB calculation as a function of the square root of the constraint variable, the rms radii of the total matter distribution. The lower panel plots in a similar fashion the BCS pairing energies for the neutron and proton sectors.

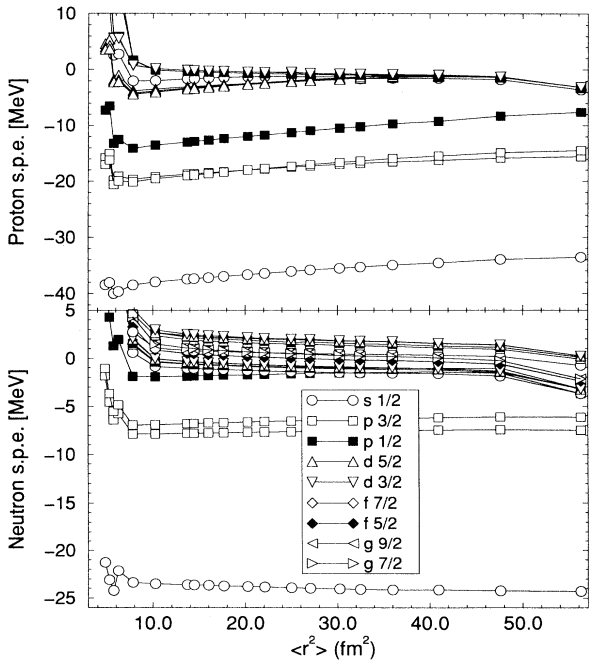

FIG. 3. The energies for some of the lowest single-particle states are plotted for the protons and neutrons in the upper and lower panels, respectively, for the constrained HFB calculation as a function of $\langle r^2 \rangle$.

levels are shown. The lowest six neutrons are almost completely contained in the $1s$ 1/2 and $1p$ 3/2 orbitals. Due to pairing correlations the last two neutrons are dispersed throughout the higher levels. There is almost no gap between the $1p$ 1/2 level and the higher levels, and for large q these levels cross. The levels higher than $2d$ 3/2 are not shown. The level density at the Fermi surface is very high, indicating that configuration mixing, i.e., the existence of correlations, is widespread.

This result is an indication that the model space required to describe the ^{11}Li GS in an extended shell model calculation is much larger than generally assumed [13]. According to the present calculation levels above the f shell surely contribute to the GS description.

In Fig. 3(b) it is clear that there is a large gap between the six inner neutrons, which represent a ^{9}Li core, and the outer two valence neutrons. The calculated occupation probabilities for the core neutrons are almost always between 1.00 and 0.99 with a minimum of $\gtrsim 0.987$. This is true for all q considered. Because of these features, a ^{9}Li core wave function can be projected out by taking the constrained HFB ^{11}Li solutions and explicitly setting the first six neutron levels to have one occupation probability and the other neutron levels to be empty. As evidenced by the fact that the core neutron probabilities are not exactly one, this is an approximate procedure, but clearly, because of the large energy gap, this should be a very reasonable representation. Let us mention that we use this procedure only for the purpose of comparing the ^{9}Li core density distribution with the free ^{9}Li one.

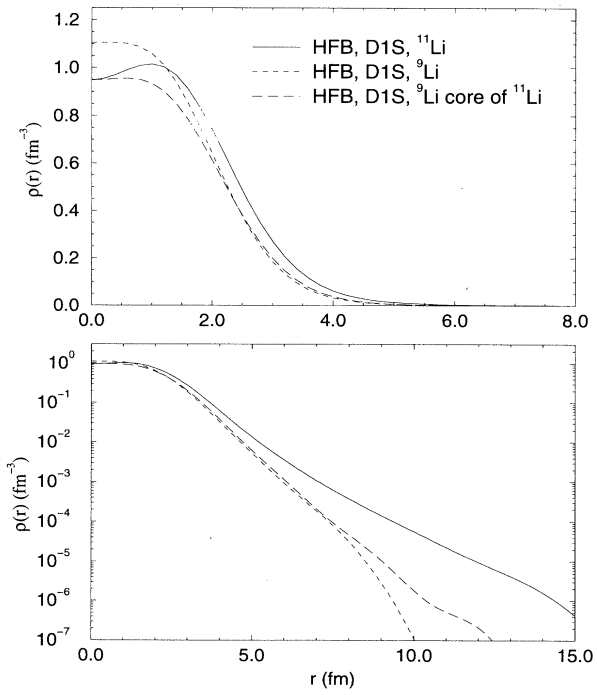

FIG. 4. The neutron radial densities for the unconstrained HFB calculation are shown as a function of r. The solid and short-dashed curves correspond to the calculated neutron densities of ^{11}Li and ^{9}Li, respectively. The long-dashed curve represents the neutron density for the ^{9}Li core projected from ^{11}Li. The lower panel is a logarithmic plot of the upper panel with the x axis extended.

In Fig. 4 the neutron density profiles are shown for the unconstrained HFB calculations of ^{9}Li and ^{11}Li, and for the ^{9}Li core projected from ^{11}Li as explained above. At the center of the nucleus the free ^{9}Li neutron density is sizably larger than the ^{9}Li core neutron density, and accordingly, the ^{9}Li core extends somewhat further in r. More precisely, the central neutron density of ^{9}Li (short-dashed curve) is about 15% larger than that of the ^{9}Li core (long-dashed curve). A similar difference was found for the protons. This is more easily seen when the tail is expanded in a logarithmic plot. The ^{11}Li core neutron density does not fall off as rapidly beyond $r = 7$ fm. Already one can see evidence, even in the simple HFB approach, for the beginning of a halolike structure. This clearly can be traced back to the fact that the extra two neutrons occupy weakly bound single-particle levels having a large spatial extension.

III. CALCULATION INCLUDING CONFIGURATION MIXING

From the evidence shown in the previous two sections it is clear that a pure single-particle model is inadequate to describe ^{11}Li. To provide a more sophisticated representation, a correlated ground state wave function is constructed as a superposition of the HFB nuclear states in the following GCM form:

$$|\chi_0\rangle = \int dq\, f_0(q)\, |\phi_q\rangle \ , \tag{2}$$

where $|\phi_q\rangle$ is a product of HFB quasiparticle states for deformation q, $f_0(q)$ is a weight function, and q is the constraint variable. In the GCM formalism a Hamiltonian kernel is constructed with the GCM wave function. By applying the variational principle, an equation is derived from which the weight functions can be calculated. A Gaussian overlap approximation (GOA), where the overlap between any two HFB states is approximated by a Gaussian in the collective variable [15], is applied to simplify these equations, deriving a Bohr Hamiltonian expression. The solution of the Bohr Hamiltonian equation gives the weight function, $f_0(q)$. These techniques have been thoroughly tested in many instances [19]. It may be that the GOA is not as accurate for smaller nuclei as in previous experience, but for the investigative study being performed here, this should be more than adequate.

The resulting ground state collective wave function, $f_0(q)$, has a corresponding total binding energy. As mentioned previously, to properly calculate the two-neutron separation energy S_{2n} one should first perform a similar collective GCM calculation for the free ^{9}Li nucleus and obtain a corresponding total binding energy. Such a calculation, somewhat beyond the scope of the present study devoted to ^{11}Li, could nonetheless be valuable since it may give indications about the relevance of the collective degrees of freedom included in the GCM method. For instance it may indicate that the present GCM calculation does not completely describe the important physics and that additional collective degrees of freedom should

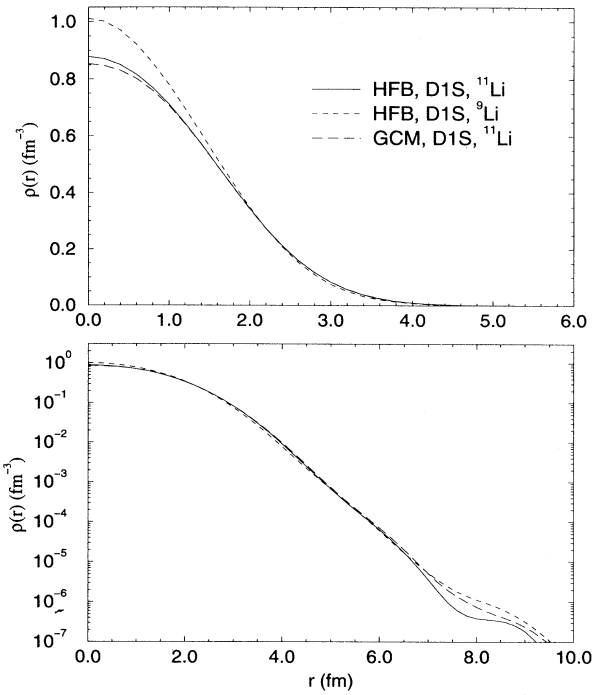

FIG. 5. The proton radial density profiles are shown as a function of r. The solid and short-dashed curves correspond to the unconstrained HFB calculation for ^{11}Li and ^{9}Li, respectively. The long-dashed curve is the result from the correlated GCM-type calculation. The lower panel is a logarithmic plot of the upper panel with the x axis extended.

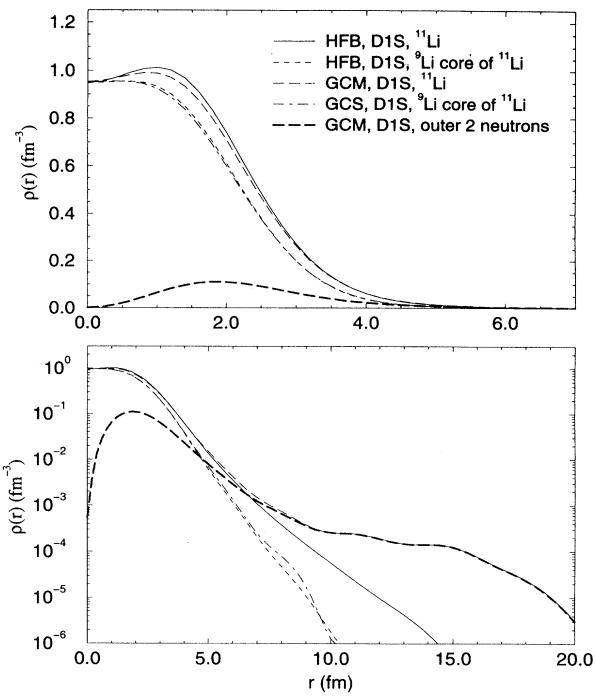

FIG. 6. The neutron radial density profiles are shown as a function of r. The solid and short-dashed curves correspond to the unconstrained HFB calculation of ^{11}Li and the projected ^{9}Li core of ^{11}Li, respectively. The long-dashed and dot-dashed curves are the result from the correlated GCM-type calculation for ^{11}Li and the projected ^{9}Li core of ^{11}Li, respectively. The shaded, fat long-dashed curve represents the difference between the long-dashed and the dot-dashed curves, thus corresponding to the two outer valence neutrons. The lower panel is a logarithmic plot of the upper panel with the x axis extended.

be included.

The ground state correlated density is calculated from (2) in the following fashion:

$$\rho_{\mathrm{GS}}(r) = \int dq' \int dq\, f_0(q') \langle \phi_{q'} | \hat{\rho}_0(r) | \phi_q \rangle f_0(q), \qquad (3)$$

where $\hat{\rho}_0(r)$ is the radial density operator obtained after angle averaging.

In Fig. 5 the proton density profile is shown from the unconstrained HFB calculation of ^{9}Li and ^{11}Li along with the GCM-type collective result for ^{11}Li. As is apparent here the ^{9}Li and ^{11}Li proton profiles are not equivalent, implying differences between the free ^{9}Li nucleus and the ^{9}Li core of ^{11}Li. The correlated ^{11}Li proton density is very similar to the uncorrelated ^{11}Li result, which should not be surprising in light of the unchanging single-particle spectrum in Fig. 3(a). For the protons the correlations have little effect upon the density distributions both near the central part and along the tail. It appears clear that there are few correlations in the ^{11}Li proton sector.

The various neutron distributions are shown in Fig. 6. As in the unconstrained HFB case an approximate representation of the ^{9}Li core can be projected out from the ^{11}Li calculation including configuration mixing. This is performed by setting the neutron occupation propabilities in the constrained HFB solutions to be either one or zero and then using these density matrices with the weight function, $f_0(q)$, obtained in the collective ^{11}Li calculation. As for the proton case the influence of correlations on the ^{9}Li core appears quite small. The collective long-range correlations represented by the GCM therefore have little effect on the ^{9}Li core as a whole.

This influence is much bigger on the full ^{11}Li neutron distribution, that is when one includes the two extra neutrons. The surface of the neutron distribution of ^{11}Li is at about $\sim$ 2.5 fm, which is much further extended than the surface of the proton distribution at $\sim$ 1.8 fm. Correlations slightly reduce this difference. Substracting the ^{9}Li core neutron distribution from the ^{11}Li neutrons gives the structure of the two valence neutrons. The two neutrons have zero density at the origin due to the Pauli blocking from the core and extend in a halolike structure. At the surface the collective valence structure causes the collective calculation to have a different neutron density profile than the unconstrained HFB neutrons.

This is most easily seen on the logarithmic plot in the lower part of Fig. 6: the HFB and GCM GS ^{11}Li neutron densities strongly differ beyond $q = 6$ fm. At this point it must be emphasized that an unphysical ledge appears

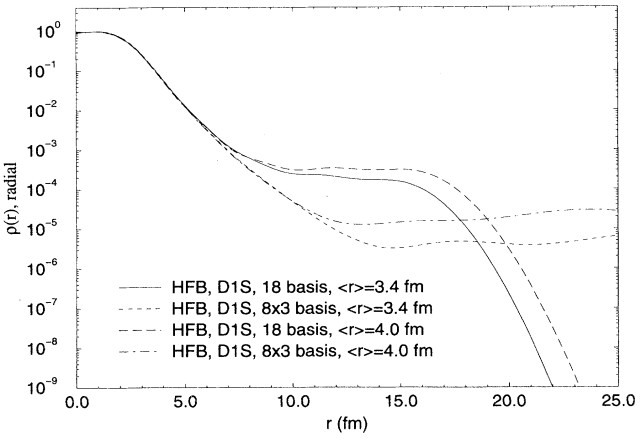

FIG. 7. The neutron radial densities are shown for the constrained HFB calculation in a logarithmic plot as a function of r. The solid and long-dashed curves correspond to calculations using a 19-shell harmonic oscillator basis, where q is constrained to 3.4^2 and 4.0^2 fm^2, respectively. The short-dashed and dot-dashed curves use three concentric eight-shell harmonic oscillators as a basis, where q is constrained to 3.4^2 and 4.0^2 fm^2, respectively.

in the GCM densities beyond $q = 7 - 8$ fm. This ledge is small in amplitude, but it affects greatly the calculated rms radius since it extends very far out. The origin of this ledge can be traced back to the structure of the HFB constrained solutions included in the configuration mixing. In Fig. 7 the neutron densities obtained in constrained HFB calculations using the 19-shell basis at $q = 3.4$ fm and $q = 4$ fm are shown. Also shown are the same results using a multioscillator spherical HFB basis. This particular multioscillator basis uses three concentric sets of eight shell bases with three different oscillator lengths. This basis corresponds to a very large single oscillator basis (≈ 60 shells). Clearly, a ledge appears in the HFB densities which depends on the basis. With the large multioscillator basis the ledge appears 2 orders of magnitude smaller and at larger r. This ledge is a result of the constraint on $\langle r^2 \rangle$, that tends to push up the density at large r, but then is restricted by the local nature of the harmonic oscillator bases. One in fact observes the parabolic fall of the densities in the 19-shell HO basis, characteristic of the HO asymptotic behavior at large r. A similar parabolic fall of the multioscillator densities is also observed at very large r (30 fm). Both the property of r^2 to be unbounded and the use of a restricted HO space may be responsible for this phenomenon.

Since there clearly exists a great deal of configuration mixing in ^{11}Li due to the radial extension of outer neutrons, one would also like to be able to extract a reasonable asymptotic tail for the GS wave function. This is necessary to get a reasonable estimate of the GS neutron rms radius. The single-particle wave functions should asymptotically be proportional to

$$\sim \frac{e^{-\kappa r}}{r}, \quad \kappa = \sqrt{\frac{-2\mu E}{\hbar^2}}, \tag{4}$$

where E is the single-particle energy. For large but finite r a polynomial in $1/r$ should be included. Therefore, one expects the HFB neutron density to behave for large r, $r > r_0$ say, as

$$\langle q|\rho(r)|q\rangle = \rho_0(q)\frac{e^{-2\alpha_q r}}{r^2}\left[1 + \frac{b_q}{r} + \frac{c_q}{r^2}\right]^2. \tag{5}$$

This form has been used to extrapolate the densities obtained in the multioscillator basis for values of r beyond the values where the unphysical ledge begins. The parameters α_q, b_q, and c_q were obtained by using a χ^2 fitting routine. $\rho_0(q)$ was chosen to match the small r density profile at r_0, where the tail was attached to the single oscillator calculation, typically at about 7 fm. The off-diagonal terms in the correlated densities (3) could then be computed from

$$\langle q'|\rho(r)|q\rangle \propto \frac{e^{-(\alpha_{q'}+\alpha_q)r}}{r^2}\left[1 + \frac{b_{q'}}{r} + \frac{c_{q'}}{r^2}\right]\left[1 + \frac{b_q}{r} + \frac{c_q}{r^2}\right]. \tag{6}$$

There is a great deal of freedom in the choice of the tail parameters and hence we were able to obtain various different parameter sets, depending on how we chose to fix things. The α_q parameters were set to be between $0.10 \rightarrow 0.15$, which corresponds to energies of about $-0.21 \rightarrow -0.47$ MeV.

With these fitted tails Fig. 8 is obtained. Different sets of fitted tail parameters are labeled by a, b, c, d, e. They give slightly but not very different values for the

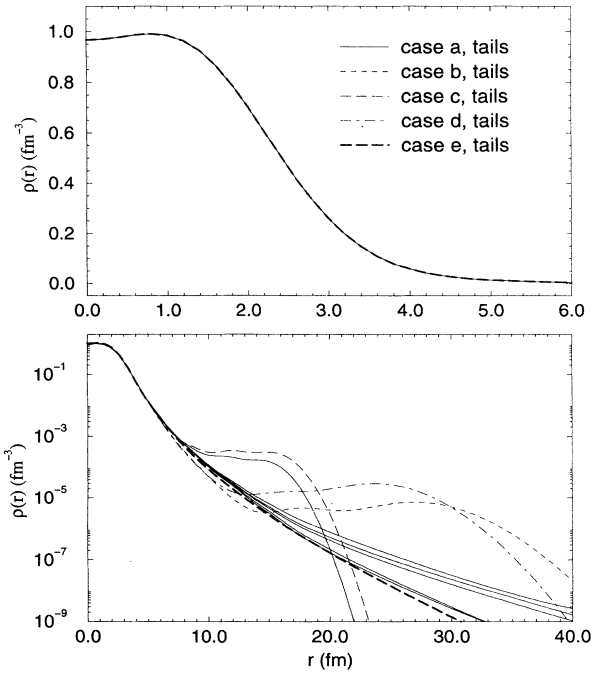

FIG. 8. The collective neutron radial densities from the GCM-type calculation are shown, where the artificial tails of various listed categories were used for the densities calculated in the constrained HFB calculations.

TABLE I. The calculated rms radii for the neutron, proton, and total matter distributions of ^{11}Li, ^{9}Li, and the ^{9}Li core projected from the ^{11}Li calculation are listed. The results from the pure mean field HFB and the correlated calculations are used.

Type of calculation	$\langle r_{\text{total}} \rangle$ (fm)	$\langle r_{\text{proton}} \rangle$ (fm)	$\langle r_{\text{neutron}} \rangle$ (fm)
^{11}Li nucleus, unconstrained HFB	2.80	2.30	2.97
^{11}Li nucleus with correlations	3.42	2.31	3.75
^{9}Li core projected from ^{11}Li in unconstrained HFB	2.55	2.30	2.67
^{9}Li core projected from ^{11}Li with correlations	2.59	2.31	2.72
^{9}Li nucleus, unconstrained HFB	2.47	2.24	2.58
^{11}Li , experiment [7]	3.12(0.16)	2.88(0.11)	3.21(0.17)
^{9}Li , experiment	2.32(0.02)	2.18(0.02)	2.39(0.02)

extrapolated density above 10^{-6}. Note that here the tails extend further out than for the unconstrained HFB case.

Let us now turn to the results concerning the rms radii. In Table I the rms radii for the various densities of Figs. 4, 5, and 6 are shown. The correlations change the calculated rms radii for the ^{9}Li core by only about 2%, which is consistent with the previous observation that correlations have a negligible effect upon the core. In this change the tail correction made above plays almost no role. As to the differences in the rms radii between the ^{9}Li nucleus and the values calculated for the ^{9}Li core, they are about 5% for both the protons and the neutrons. This effect upon the rms radius appears to be small, but the comparison of the density distributions made in the previous section yields a more pronounced difference. One may say that the ^{9}Li system is slightly inflated when two extra neutrons are added. This comparison assumes that the ^{9}Li nucleus ground state wave function is not significantly influenced by correlations, which certainly is reasonable in view of the insensitivity of correlations on the ^{9}Li core. Again, the comparisons made for the nine-nucleon systems do not depend on the tail correction introduced previously. One may conclude that in this many-body calculation of ^{11}Li there appears to exist a substantive ^{9}Li core which notably differs from a free ^{9}Li nucleus. One expects that these differences may have a non-negligible effect upon the mean field felt by the two outer neutrons.

Going to the full ^{11}Li rms radii, the value listed in Table I with correlations included, but without tail correction (3.42 fm), clearly is overestimated. In Table II the rms radii obtained without and with the various parametrized tail corrections are listed. The largest $\langle r_{\text{rms}} \rangle_{\text{tot}}$ using a fitted tail is case *a* with 2.88 fm. In the calculations performed here, the increase in rms radii due to correlations is between $\sim 0.04 \rightarrow 0.08$ fm with realistic tails. This result is somewhat disappointing in view of the amount of complexity put into the GS wave functions. The total and neutron rms radii, although not far from being consistent with the experimental error bars, appear 0.2 fm smaller than the nominal experimentally extracted values.

At this point, one may note that the present radius results probably represent lowest values. In fact, when using the multioscillator basis the resulting potential energy surface appears somewhat flatter than the 19-shell basis shown in Fig. 1. This indicates a fully realistic calculation, where density tails would be correctly described, would also yield a much softer collective potential and therefore a stronger configuration mixing. Hence effects of correlations larger than those derived here, especially with respect to the rms radius predictions, would certainly be found.

It should be realized that since the proton sector was calculated with a blocking approximation, the ground state spin of the nucleus has been artificially set. In Table III calculated axial proton quadrupole moments

TABLE II. The calculated rms radii in fm for the neutron, proton, and total matter distributions of ^{11}Li including correlations are tabulated using various fitted asymptotic tails.

With fitted tail	$\langle r_{\text{tot}} \rangle$	$\langle r_{\text{prot}} \rangle$	$\langle r_{\text{neut}} \rangle$
^{11}Li nucleus, HFB	2.80	2.30	2.96
^{11}Li with correlations	3.42	2.31	3.75
^{11}Li case *a*	2.88	2.31	3.07
^{11}Li case *b*	2.84	2.31	3.02
^{11}Li case *c*	2.85	2.31	3.03
^{11}Li case *d*	2.86	2.31	3.04
^{11}Li case *e*	2.87	2.31	3.05

TABLE III. The calculated axial quadrupole moments in millibarns for the neutron, proton, and total matter distributions of ^{11}Li, ^{9}Li, and the ^{9}Li core projected from ^{11}Li calculation are listed. The results from the axial HFB and GCM calculations are used.

Type of calculation	$\langle Q_{20}^{\text{proton}} \rangle$ (mb)	$\langle Q_{20}^{\text{neutron}} \rangle$ (mb)
^{11}Li unconstrained HFB	-31.20	-11.08
Correlated GCM ^{11}Li	-31.13	2.87
^{9}Li core projected from ^{11}Li unconstrained HFB	-31.20	-54.94
^{9}Li core projected from correlated GCM ^{11}Li	-31.13	-53.76
Free ^{9}Li, HFB, *D1S*	-43.46	-96.24
^{11}Li, experiment [20]	-31.2 (4.5)	
^{9}Li, experiment [20]	-27.4 (1.0)	

$\langle Q^p_{20} \rangle$ are displayed for ^{11}Li, the ^{9}Li core, and the free ^{9}Li. The HFB and correlated GCM calculations are seen to give approximately the same charge quadrupole moment for ^{11}Li and for the ^{9}Li core. This feature indicates that the proton sector is not greatly affected by correlations in ^{11}Li. The calculated value is in remarkably close agreement with the experimental result well within the experimental error. Concerning the free ^{9}Li, it is seen that HFB overpredicts by a factor of almost 2 the experimental result. This shows that configuration mixing involving for instance $1p$ 1/2 proton states certainly would be important for reproducing $\langle Q^p_{20} \rangle$ in ^{9}Li. As an indication of the sensitivity of this quantity to the model used in ^{9}Li, let us mention that performing the blocked HFB calculation in spherical symmetry instead of axial symmetry changes $\langle Q^p_{20} \rangle$ from -43.5 mb to -20.4 mb. In the case of ^{11}Li, a similar HFB calculation increases the value -31.20 mb given in Table III to only -29.2 mb.

IV. CONCLUSIONS

A microscopic many-body approach of the ground state stucture of ^{11}Li is presented. Correlations beyond the mean field are introduced by means of a GCM-type configuration mixing of constrained HFB states. The constraint employed is the mean square nuclear radius. The long-range correlations included here therefore are those associated with a change in the nuclear volume. The sole input into the calculation is the well-tested, finite-range *D1S* effective interaction introduced by *Gogny*, which has been devised in order to account for both the average and pairing fields in nuclei. For this reason, pairing correlations are included in the constrained HFB approach in a completely parameter-free manner.

It is found that the long-range correlations taken into account are restricted almost exclusively to the sector occupied by the two valence neutrons. The correlations have a significant effect and play an important role in describing ^{11}Li. The ^{11}Li experimental proton quadrupole moment is remarkably well reproduced. The GCM mixing calculation yields a correlated GS wave function with a very large $\langle$rms$\rangle$ radius (3.42 fm) which is found to be mainly unphysical due to difficulties associated with the description of HFB quasiparticle states at large distance. When corrections are made to recover proper asymptotic behaviors, the obtained $\langle$rms$\rangle$ radius falls in the range 2.84–2.88 fm, which is somewhat smaller than the 3.12 ± 0.16 fm deduced from experiment. Although this result probably represents a conservative figure, one may conclude that the kind of correlations included here do not fully account for the observed ^{11}Li halo.

By separating out the six most bound neutrons in ^{11}Li, a well-defined ^{9}Li core can be recovered, whose structure is almost independent of the amount of correlations introduced in ^{11}Li. Although the $\langle$rms$\rangle$ proton and neutron radii of the ^{9}Li core found in this way appear close to those of a free ^{9}Li nucleus, there is a significant difference in the matter density profile of the two systems. Namely the central density of the former is depressed by about 15%. This figure does not appear to depend on the detailed procedure adopted to define the ^{9}Li core. These results clearly support the three-body picture of ^{11}Li. They also clearly indicate that the underlying ^{9}Li core of ^{11}Li cannot be identified with the GS of a free ^{9}Li nucleus.

Finally let us mention that the difficulties encountered in describing the large distance behavior of quasiparticle states could not be completeley alleviated with the use of a multioscillator basis with three oscillator lengths. It seems in this respect that an accurate *ab initio* description of the structure of halo nuclei, and more generally of drip line nuclei, requires one to extend considerably the numerical techniques presently employed. One way to do this would be for instance to make use of the collocation basis-spline technique [21] in a very large spatial box.

ACKNOWLEDGMENTS

One author (C.R.C) would like to acknowledge the gracious hospitality of the Service de Physique et Technique Nucléaires at the Centre d'Etudes de Bruyères-le-Chaâtel, where much of this work was performed. This research was performed in part under the auspices of the U.S. Department of Energy under Contracts No. DE-AC05-84OR21400 with Martin Marietta Energy Systems, Inc., and No. DE-FG05-87ER40376 with Vanderbilt University. This research was supported in part by the U.S. Department of Energy, Office of Scientific Computing.

[1] M. V. Zhukov, B. V. Danilin, D. V. Fedorov, J. M. Bang, I. J. Thompson, and J. S. Vaagen, Phys. Rep. **231**, 151 (1993).
[2] J. M. Bang, I. J. Thompson, M. V. Zhukov, B. V. Danilin, D. V. Fedorov, and J. S. Vaagen, Niels Bohr Institute Report No. NBI-91-31, 1991; J. M. Bang and I. J. Thompson, Phys. Lett. B **279**, 201 (1992).
[3] Y. Tosaka and Y. Suzuki, Nucl. Phys. **A512**, 46 (1990).
[4] A. S. Jensen and K. Riisager, Nucl. Phys. **A537**, 45 (1992).
[5] L. Johannsen, A. S. Jensen, and P. G. Hansen, Phys. Lett. B **244**, 357 (1990); P. G. Hansen and B. Jonson, Europhys. Lett. **4**, 409 (1987).
[6] A. C. Hayes, Phys. Lett. B **254**, 15 (1991).
[7] I. Tanihata, T. Kobayashi, O. Yamakawa, S. Shimoura, K. Ekuni, K. Sugimoto, N. Takahashi, and T. Shimoda, Phys. Lett. B **206**, 592 (1988).
[8] R. Anne *et al.*, Phys. Lett. B **250**, 19 (1990); K. Riisager *et al.*, Nucl. Phys. **A540**, 365 (1992).
[9] H. Sato and Y. Okuhara, Phys. Lett. B **162**, 217 (1985); G. F. Bertsch, B. A. Brown, and H. Sagawa, Phys. Rev. C **39**, 1154 (1989); W. Koepf, Y. K. Gambhir, P. Ring,

and M. M. Sharma, Z. Phys. A **340**, 119 (1991).
[10] H. Sagawa, Phys. Lett. B **286**, 7 (1992).
[11] Z. Y. Zhu, W. Q. Shen, Y. H. Cai, and Y. G. Ma, Phys. Lett. B **328**, 1 (1994).
[12] G. F. Bertsch and H. Esbensen, Ann. Phys. (N.Y.) **209**, 327 (1991).
[13] T. Hoshino, H. Sagawa, and A. Arima, Nucl. Phys. **A506**, 271 (1990).
[14] N. A. F. M. Poppelier, L. D. Wood, and P. W. M. Glaudemans, Phys. Lett. B **157**, 120 (1985); A. C. Hayes and D. Strottman, Phys. Rev. C **42**, 2248 (1991); J. M. G. Gomez, C. Prieto, and A. Poves, Phys. Lett. B **295**, 1 (1992).
[15] P. Ring and P. Schuck, *The Nuclear Many-Body Problem* (Springer-Verlag, New York, 1980).
[16] J.-F. Berger, J.-Dechargé, and D. Gogny, *Proceedings of the International Workshop on Nuclear Structure Models*, Oak Ridge, Tennessee, 1992 (World Scientific, River Edge, NJ, 1992).
[17] J. Dechargé and D. Gogny, Phys. Rev. C **21**, 1568 (1980).
[18] S. Cohen and D. Kurath, Nucl. Phys. **73**, 1 (1965); D. Kurath, Phys. Rev. **140**, B1190 (1965).
[19] C. R. Chinn, J.-F. Berger, D. Gogny, and M. S. Weiss, Phys. Rev. C **45**, 1700 (1992).
[20] E. Arnold, J. Bonn, A. Klein, R. Neugart, M. Neuroth, E. W. Otten, P. Lievens, H. Reich, W. Widdra, and ISOLDE Collaboration, Phys. Lett. B **281**, 16 (1992).
[21] C. de Boor, *A Practical Guide to Splines* (Springer-Verlag, New York, 1978); C. R. Chinn, A. S. Umar, M. Vallières, and M. R. Strayer, Phys. Rev. E **50**, 5096 (1994).